Highly Dispersible Hexagonal Carbon-MoS_2-Carbon Nanoplates with Hollow Sandwich Structures for Supercapacitors

Ting Quan,[a] Nicolas Goubard-Bretesché,[b] Eneli Härk,[a] Zdravko Kochovski,[a] Shilin Mei,[a] Nicola Pinna,[b],[c] Matthias Ballauff,[a],[c],[d] Yan Lu*[a],[c],[e]

Abstract: MoS_2, a typical layered transition metal dichalcogenide is promising as an electrode material in supercapacitors. However, its low electrical conductivity could lead to limited capacitance when applied in electrochemical devices. Here, a new nanostructure made of hollow carbon-MoS_2-carbon was successfully synthesized by a L-cysteine assisted hydrothermal method using gibbsite as a template and polydopamine as a carbon precursor. After calcination and etching of the gibbsite template, uniform hollow platelets, which are made of a sandwich-like assembly of the partial graphitic carbon and the two-dimensional layered MoS_2 flakes, were obtained. The platelets showed excellent dispersibility and stability in water and good electrical conductivity due to the carbon provided by the calcination of the polydopamine coatings. The hollow nanoplate morphology of the material provided a high specific surface area of 543 m^2/g, a total pore volume of 0.677 cm^3/g and fairly small mesopores (~5.3 nm). The material was applied in a symmetric supercapacitor and exhibited a specific capacitance of 248 F/g (0.12 F/cm^2) at a constant current density of 0.1 A/g, suggesting that the hollow carbon-MoS_2-carbon nanoplates are promising candidate materials for supercapacitors.

Introduction

In recent years, substantial research efforts have been devoted to layered transition metal dichalcogenides (TMD) for broad applications such as catalysis, electrochemistry, and optics. [1] Among all, MoS_2, a typical TMD material, has gained much attention.[2] MoS_2 has a layered structure, each layer is made of MoS_6 trigonal prisms which share edges with each other. The layers are kept together by weak Van der Waals interactions between sulfide ions. Mono- or few-layered MoS_2 can provide a high specific surface area and an extended contact with an electrolyte when it is applied in energy storage devices. Thus, MoS_2 has been widely studied as promising anode materials in lithium ion batteries (LIBs) and sodium ion batteries (SIBs) due to their low cost, high specific capacity, and layered structure with improved intercalation and de-intercalation dynamics of alkaline ions. Recently, metallic 1T-MoS_2 phase has been demonstrated as a highly efficient electrode material for supercapacitors, which in particular are an ideal technology to exploit the beneficial properties of 2D materials.[3] [4]

Up to now, there are two typical methods to synthesize MoS_2[5]: the top-down method (liquid phase exfoliation)[5d] and the bottom-up method (wet chemical synthesis)[6]. In order to control the size and shape of the particles, many researchers prefer to use the chemical synthesis, which shows advantages such as an easy control of size and shape of particles.[7] Recently, Lou *et al*.[8] fabricated MoS_2 microboxes by an L-cysteine assisted hydrothermal method using $MnCO_3$ microcubes as a template and applied it as an anode material for lithium-ion batteries. Ilanchezhiyan *et al*.[9] synthesized sphere-like MoS_2 particles, which consists of MoS_2 layered structures, by a hydrothermal method for electrochemical supercapacitor applications. These MoS_2 nanostructures have been mixed with carbon black and Polyvinylidene fluoride (PVDF) (in the weight ratio of 70:20:10) to fabricate supercapacitor electrode, which exhibited specific capacitances of 122 F/g at a current density of 0.5 A/g in a three-electrode cell assembly.

Despite these promising results, there are still challenges to be overcome to apply MoS_2 as an electrode material in devices. The electrical conductivity of MoS_2 is lower than that of typical carbon materials, which can limit the electrochemical performance of the devices. Therefore, combining MoS_2 with a higher conductivity material like carbon or graphite is a good solution. For example, Kamila *et al*.[10]synthesized a hybrid material combining MoS_2 hollow spheres (MoS_2-HS) and with reduced graphene oxide (rGO/MoS_2-HS) for supercapacitor applications. The rGO/MoS_2 showed enhanced gravimetric capacitance values with higher specific energy/power outputs and better cyclic performance than pure MoS_2-HS. Ren *et al*.[11] succeeded to grow polyaniline (PANI) nanowire arrays on both the external and internal surfaces of 3D tubular MoS_2 by in situ oxidative polymerization of aniline monomers. The obtained hybrid material combines the double-layer capacitance of MoS_2 with the battery-type Faradaic contribution of PANI. Therefore, compared to MoS_2, the overall capacity of the electrodes was increased.

Because of the interlayer van der Waals attraction and their high surface energy, the MoS_2 layers tend to aggregate not only

[a] T. Quan, Dr. E. Härk, Dr. Z. Kochovski, Dr. S. Mei, Prof. M. Ballauff, Prof. Y. Lu
Soft Matter and Functional Materials
Helmholtz-Zentrum Berlin für Materialien und Energie
Hahn-Meitner-Platz 1, 14109 Berlin, Germany
E-mail:yan.lu@helmholtz-berlin.de
[b] Dr. N. Goubard-Bretesché, Prof. N. Pinna
Institut für Chemie
Humboldt-Universität zu Berlin
Brook-Taylor-Str.2, 12489 Berlin, Germany
[c] Prof. N. Pinna, Prof. M. Ballauff, Prof. Y. Lu
IRIS Adlershof
Humboldt-Universität zu Berlin
Zum Großen Windkanal 6, 12489 Berlin, Germany
[d] Prof. M. Ballauff
Institut für Physik
Humboldt-Universität zu Berlin
Newtonstraße 15, 12489 Berlin, Germany
[e] Prof. Y. Lu
Institute of Chemistry
University of Potsdam
14467 Potsdam, Germany

Supporting information for this article is given via a link at the end of the document.

during the synthesis but also during charge-discharge cycling of supercapacitors, leading to limited capacitance and low stability. It has been suggested that assembling MoS_2 layers perpendicularly onto a support will provide 2D materials with a large specific surface area and highly exposed active sites.[8, 12] In addition, the existence of the support will avoid the aggregation of the particles, thus improving the durability of the electrode.[13] Moreover, to further improve the contact of the interface electrolyte/active material, providing additional electrochemically active sites,[14] a hollow structure can be synthesized, for example by growing MoS_2 onto a template, which is subsequently removed.[8, 15] Until now, only spherical or cube-like MoS_2 hollow structures have been reported. The design and synthesis of two dimensional hollow MoS_2 particles based on template-assisted method still remain a significant challenge. It has been already extensively reported that MoS_2 can been deposited onto graphene or carbon materials,[16] but carbon or graphene cannot be removed to generate MoS_2 hollow particles.

Recently we have reported the use of an easy-removable and well-defined template (gibbsite nanoplatelets) to synthesize hollow nanostructures.[17] The hexagonal nanoplate shaped template could deliver a high specific surface area of the material and the hollow structure from it can better withstand the volume change during cycling when applied in energy storage devices. S. Ding *et al.* have reported the use of hollow SnO_2@carbon nanosheets as anode for lithium-ion batteries. As they have shown, the structure of hollow carbon nanosheets contributes to the improvement of the capacity and stability of the SnO_2 anode material.[18] In this work, we report a multistep strategy to synthesize hollow carbon-MoS_2-carbon hybrid nanoplates by the L-cysteine assisted hydrothermal method in the presence of sodium molybdate using gibbsite as the template and polydopamine (PDA) as the carbon precursor, as

Figure 1. Schematic representation of the synthesis route to prepare hollow carbon-MoS_2-carbon hybrid nanoplates.

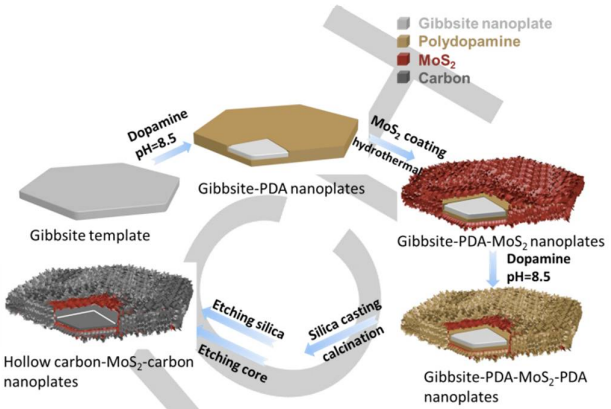

shown in Figure 1. By removing the gibbsite template, the final product exhibits a hollow hexagonal nanoplate structure with high specific surface area and excellent dispersibility in water. The sandwich-like structure with MoS_2 in the middle and partial graphitic carbon on both sides has a much higher conductivity and better dispersibility than that of bulk MoS_2, which is much better to be applied in supercapacitors. In addition, the hollow structure of carbon-MoS_2-carbon with well-defined interior voids can prevent the volume change during charging and discharging of supercapacitors, mainly caused by the intersheet and intrasheet double layer storage.[19]

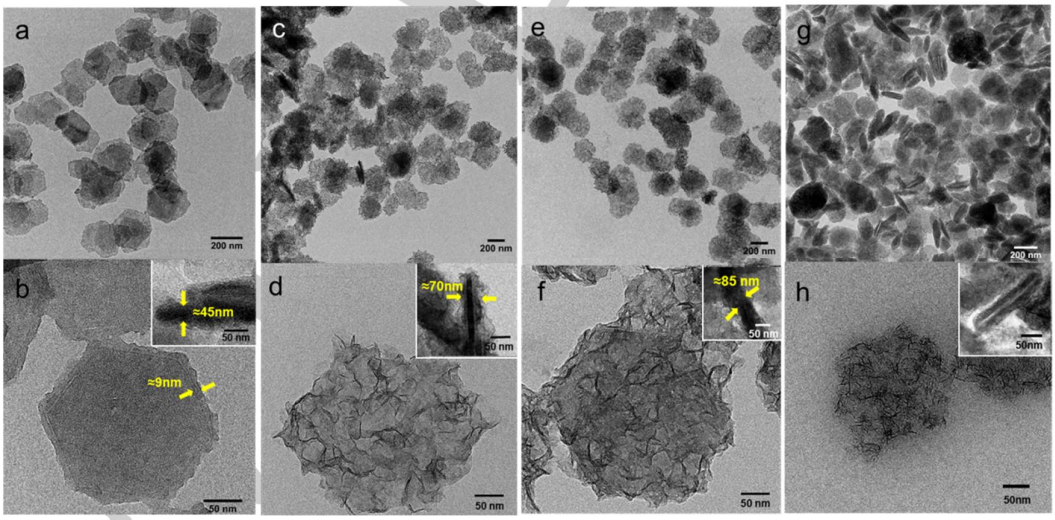

Figure 2. (a and b) TEM images of the polydopamine-coated gibbsite nanoplates, thickness of the polydopamine layer ≈9 nm. (c and d) TEM images of the gibbsite-PDA-MoS_2 nanoplates. (e and f) TEM images of the gibbsite-PDA-MoS_2-PDA nanoplates. (g and h) TEM images of the hollow carbon-MoS_2-carbon nanoplates. Insets: standing nanoplates, which indicates the thickness and structures of the nanoplates.

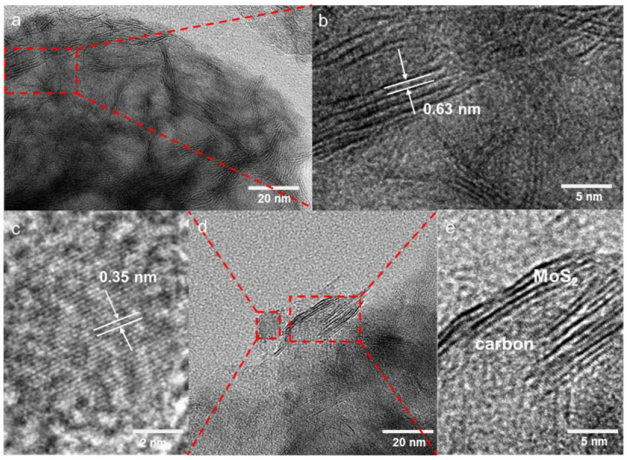

Figure 3. (a and d) HR-TEM images of the enlarged domain in the hollow carbon-MoS_2-carbon nanoplates, which indicates the layered structure of MoS_2 and graphite-like carbon. (b, c and e) HR-TEM images of the parts indicated in (a and d). The interlayer distances of MoS_2 and carbon in the hybrid nanoplates are 0.63 nm and 0.35 nm, respectively.

Results and Discussion

Figures 2(a) and (b) show the TEM images of the polydopamine-coated gibbsite nanoplates. The thickness of the polydopamine shell was about 9 nm. Then a MoS_2 layer was grown on the uniform core through an L-cysteine assisted hydrothermal method.[20] Here, Na_2MoO_4 and L-cysteine were used as Mo and S sources, respectively. During the hydrothermal process, the functional groups (-SH, $-NH_2$, $-COO^-$) of L-cysteine could conjugate with PDA and Mo-containing ions, thus promoting the nucleation of MoS_2 on the template.[8, 20-21] It can be seen from Figure 2 (d) that the nanoplates can keep the same shape as the template (Figure S1) and they are composed of well-arranged MoS_2 nanosheets. The thickness of the whole MoS_2-coated gibbsite-PDA nanoplates is about 70 nm, indicating that the MoS_2 layer is quite thin (about 13 nm). In order to improve the conductivity of the material, another layer of polydopamine was coated on the nanoparticles, increasing the whole thickness to about 85 nm. As a next step, a dense silica matrix was synthesized to confine individual gibbsite-PDA-MoS_2-PDA and obtain dispersible nanoparticles. The silica nanocasting technique can be referred to our previous work.[17] After carbonization at 700°C under argon, monodispersed hollow carbon-MoS_2-carbon nanoplates were obtained by the elimination of the gibbsite cores and silica portion by acid etching for several days. The TEM images in Figure 2(g) and 2(h) demonstrate the well-defined shape of the hollow carbon- MoS_2-carbon nanoplates with ideal dispersibility. The obtained particles show uniform hollow structure as seen from the TEM image of the standing nanoplate particle and keep the same shape as the gibbsite templates with a shell thickness of about 22 nm.

To further study the structure and morphology of our materials, HR-TEM measurements of the hollow carbon-MoS_2-carbon nanoplates were performed. As shown in Figure 3(a), (d) and (e), the layered structures of MoS_2 and graphitized carbon co-exist at the same time and are embedded each other in the hybrid material. It clearly demonstrates that the layer structure of MoS_2 is uniformly distributed in the carbon sheet. From Figure 3(b), few layers of MoS_2 showing the typical interlayer spacing of about 0.63 nm could be observed, indexed to the (002) plane of hexagonal phase of MoS_2. This indicates that the hollow carbon-MoS_2-carbon nanoplates maintain the thin-layered structure of MoS_2, which will be essential for their electrochemical performance. In Figure 3(c), the graphitic phase of carbon part is shown with the interlayer spacing of about 0.35 nm, which agrees well with the previous reports.[22] Such 2D hollow nanoplate-structure of MoS_2 coated with carbon on both sides features better conductivity than that of pure MoS_2.

The photograph of the as prepared hollow carbon-MoS_2-carbon dispersion in water is shown in Figure 4(a), indicating that the nanoparticles could form a stable colloidal suspension in water under neutral pH condition for more than 24 hours. It is expected that the surface of the nanoplates is charged as supported by zeta potential measurements carried out in our previous work.[17] Therefore, despite there is no surfactant applied to disperse the particles, the electrostatic repulsion between the surface charged carbon coating, generated from the carbonization of polydopamine, provides the well stabilization of nanoplates.[23] In order to study the structure of the materials after each synthesis step, XRD measurements were performed. As shown in Figure S2 in the supporting information, the reflections at 2θ = 18.3°, 20.4° and 30.2° correspond to the (002) (100) and (004) planes of the gibbsite template, respectively. The peaks centered at 2θ = 32.6° and 56.7° correspond to the 100 and 110 reflections of 2H-phase of MoS_2. The asymmetric shape of the 100 reflection, with a rapid increase on the low angle side and a long tail on the

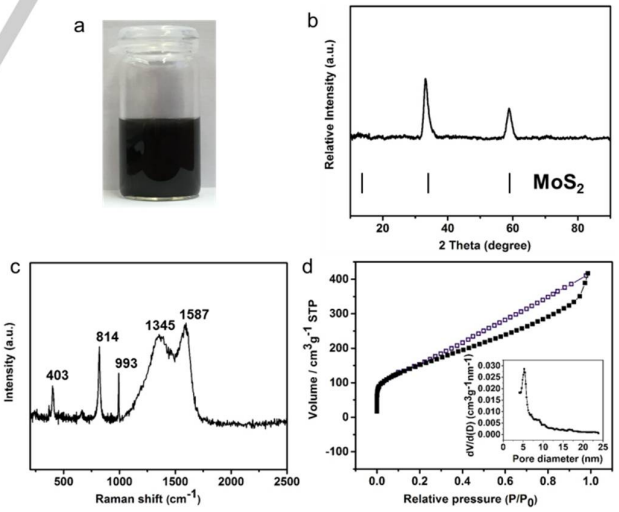

Figure 4. (a) Photograph of the hollow carbon-MoS_2-carbon nanoplates dispersed in water. (b) XRD patterns of the hollow carbon-MoS_2-carbon nanoplates. (c) Raman spectra, and (d) Nitrogen adsorption and desorption isotherms of the hollow carbon-MoS_2-carbon nanoplates. The inset shows the pore size distributions obtained using the Barrett-Joyner-Halenda (BJH) method.

high angle side, meets the feature of 2D crystals in XRD patterns.[24] The 002 reflection of MoS_2 at 2θ = 14° is extremely weak, suggesting that the stacking of the MoS_2 layers along the c-axis is limited to only a few layers as also supported by HRTEM images in Figure 3.[10] After the etching of the cores, the diffraction peaks of gibbsite disappear totally in the final hollow carbon-MoS_2-carbon nanoplates as shown in Figure 4(b), which proves again that the template is completely removed. The two peaks at 2θ = 32.6° and 56.7° of MoS_2 become more narrow and obvious in the final product, indicating that the crystallinity of MoS_2 is better after annealing. No peak of carbon was detected because of the small amount of carbon in the final product.[25] The hollow carbon-MoS_2-carbon nanoplate sample was further studied by Raman spectroscopy in resonant conditions (633 nm). In Figure 4(c), the nanoparticles show the characteristic bands at 377 cm^{-1} and 403 cm^{-1} corresponding to the in plane E^1_{2g} and out of plane A^1_g vibration modes of MoS_2.[10, 26] The additional peaks at 814 cm^{-1} and 993 cm^{-1} should be the terminal stretching vibration of Mo=O which results from the exposure to the air of MoS_2 during etching process or when stored.[10] Additionally, there are another two bands at 1345 cm^{-1} and 1587 cm^{-1} which are assigned to the D and G bands of sp^2 carbon. D is taken as the disordered band and G is the in plane stretching motion between sp^2 carbon atoms.[27] To further investigate the elemental composition of the nanoparticles, a Thermogravimetric analysis (TGA) is further applied. MoS_2 is oxidized to MoO_3 in O_2 flow. The formation of MoO_3 from MoS_2 and CO_2 from carbon occurs in the same temperature range of 300-400 °C, leading to a mass loss of 38%. Then the weight fraction of carbon in the initial sample is calculated to 31.7%.[28] Nitrogen adsorption and desorption isotherms of the hollow carbon- MoS_2-carbon nanoplates are presented in Figure 4(d) and reveal that the Brunauer-Emmet-Teller (BET) surface area[29] is about 543 m^2/g with the pore volume of 0.677 cm^3/g. The pore size distribution was evaluated from the desorption curve of the nitrogen isotherms using the Barrett-Joyner-Halenda (BJH) model[30] and indicates that the material is mesoporous with a pore size of about 5.3 nm. The hollow

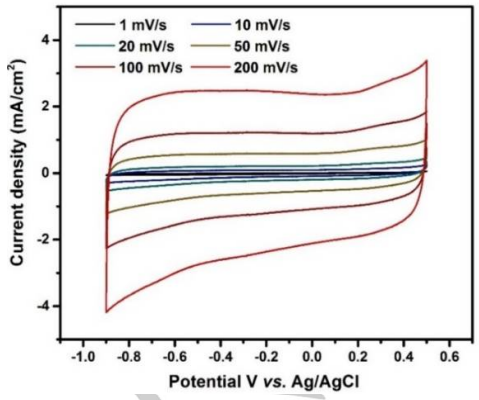

Figure 5. Cyclic voltammetry curves of the hollow carbon-MoS_2-carbon material in a three-electrode cell in 1M Li_2SO_4 aqueous electrolyte solution at different scan rates.

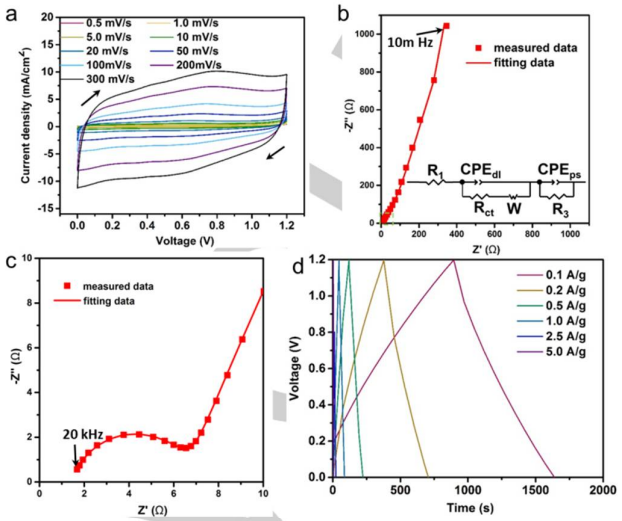

Figure 6. (a) CV profiles at different scan rates from 0.5 mV/s to 300 mV/s, (b) Nyquist plots measured within frequency range from 20 kHz to 10 mHz. (The inset is the equivalent circuit which is employed to fit the impedance spectra.[31] The dotted line is measured data and solid line fitting data), (c) the close-up view at the high frequency of the Nyquist plots, and (d) galvanostatic charge/discharge curves of the symmetric supercapacitor with hollow carbon-MoS_2-carbon nanoplates as electrode material at different current densities.

carbon-MoS_2-carbon nanoplates show higher BET surface area than that of pure carbon nanoplates (~460 m^2/g).[17]

As mentioned before, the hollow structure and large interlayer spacing of MoS_2 could promote the diffusion of the electrolyte ions in the structure of the material, providing good electrochemical performance. In this work, the prepared hollow carbon-MoS_2-carbon nanoplates were used as electrode material for supercapacitors. The working mechanism of supercapacitors based on MoS_2 thin films as electrode materials includes three modes[19]: (i) intersheet double-layer charge storage, (ii) intrasheet double-layer charge storage on individual atomic MoS_2 layers through diffusion into the basal edges, and (iii) faradaic charge transfer process on the Mo center, which can exhibit oxidation states varying from +2 to +6. The electrochemical properties of our material were first investigated by cyclic voltammetry in a three-electrode configuration, using a 1M Li_2SO_4 solution as electrolyte. The electrochemical potential window was varied from -0.9 V to 0.5 V vs. Ag/AgCl and the corresponding current density is plotted on Figure 5. At different

scan rates, the CV curves are close to rectangular shape, indicating the electrical double layer capacitor (EDLC) type system, which is attributed to the diffusion of the electrolyte ions into the intersheet and intrasheet of MoS_2.[19] With the increasing of the scan rate, CV curves keep their rectangular shape, showing a good high-rate performance. The beginning of the redox peaks can be observed from 0.3 V vs. Ag/AgCl in anodic scan and -0.7 V vs. Ag/AgCl in cathodic scan, which is attributed to the decomposition of our aqueous electrolyte.[32]

To calculate the energy density as well as the power density (according to eqs. (2) and (3)) of the hollow carbon-MoS_2-carbon nanoplates in a supercapacitor, a symmetric two-electrode cell

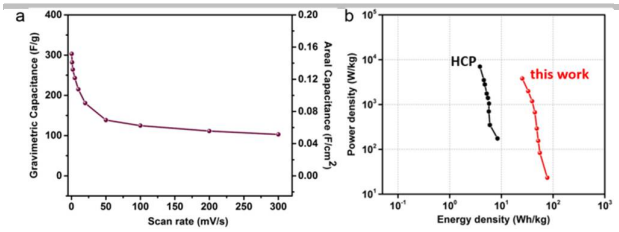

Figure 7. (a) Plot of specific capacitance of the C-MoS_2-C material vs. the scan rate. (b) Ragone plot of energy density vs. power density of the hollow carbon-MoS_2-carbon nanoplates and comparison with hollow carbon nanoplates (HCP), obtained using the same templating method.[17] Gravimetric values are reported per mass of active material in one electrode.

was tested. To moderate the electrolyte decomposition observed during the preliminary three electrode measurements, the voltage range was set to 1.2 V. The CV curves for different scan rates are presented in Figure 6(a). A quasi-rectangular shape of CV curves has been observed, which is characteristic of the electrochemical double-layer capacitance behaviour. In addition, there are two reversible peaks at 0.6 V and 0.8 V attributed to the pseudocapacitive behaviour of MoS_2. There are close relationships between the oxidation/reduction peaks and the oxidation modification of Mo atoms in the MoS_2 layers, which ranges from +2 to +6.[33] Additionally, there is a broad hump at 0.8 V during charging and a hump at 0.6 V during discharging, attributed to the pseudocapacitive behavior of MoS_2. Furthermore, with the increasing of the scan rate, the CV curve shape is maintained, denoting a stable capacitive behaviour. We attribute this effect to i) the hollow nanoplate morphology ensuring an easy diffusion of the electrolyte and ii) to the low resistivity of the MoS_2/carbon nanocomposite.[34] The Nyquist plot obtained for two electrode system as described in electrochemical measurement Section is given in Fig. 6b. The impedance was measured at open circuit voltage within frequency range from 20 kHz to 10 mHz. The impedance data reveal nearly ideal capacitive behaviour at low frequencies influenced slightly by the ion diffusion process within the active electrode material (Figure 6(b)). Obtained semi-circle at high-frequencies due to the charge transfer resistance at the electrode-electrolyte interface (R_{ct}) is demonstrated in Fig.6 (c). Our findings agree well with the results presented by Ren *et al.*.[11] The equivalent circuit presented in Figure 6(b) has been applied to fit the measured data. The observed semi-circle was reproducible and fitted data agree well with the measured one as demonstrated in Figure 6 (b) and (c). The goodness of the fit χ^2 and other fitting parameters are given in Supporting Information in Table S1. The bulk electrolyte solution resistance R_1 and the charge transfer resistance R_{ct} for the studied system is found to be 1.5 Ω and 4.7 Ω, respectively, indicating that our hollow nanoplates not only exhibit good conductive capability due to the carbon coating, but also provide good diffusion of the electrolyte ions into the electrode material.[35] The specific capacitance of the symmetric supercapacitor was determined by galvanostatic charge-discharge measurement (Figure 6(d)) at various current densities. The obtained curves display the expected triangle shape of a capacitive material, and there is no obvious ohmic potential (IR) drop (the voltage drop due to the energy losses) during discharging. The capacitance values of the supercapacitor with 1M Li_2SO_4 in H_2O as an electrolyte decrease from 248 F/g (0.12 F/cm^2) to 178 F/g (0.09 F/cm^2) when the current density increases from 0.1 A/g to 1.0 A/g, as calculated from the galvanostatic charge/discharge curves (all calculated capacitance values are shown in Table S2 in the supporting information). Table 1 lists the capacitance

Table 1. Summary of the present and reported data of MoS_2 or carbon related materials for symmetric supercapacitors. The capacitance values are presented per mass of active material, along with the mass loadings of the electrodes.

Sample	Binder	Electrolyte	Mass loading	Capacitance	Ref.
2D layered MoS_2-rGO hybrids	Nafion	1.0 M Na_2SO_4	2 mg/cm^2	190 F/g (1 A/g)	[10]
MoS_2 hollow spheres	Nafion	1.0 M Na_2SO_4	2 mg/cm^2	97.5 F/g (1 A/g)	[10]
MoS_2 sponge material	PVDF	0.5 M H_2SO_4	5 mg/cm^2	90.1 F/g (1 A/g)	[36]
2D exfoliated MoS_2/CNT hybrid ink	Binder free	PVA-H_2SO_4	1 mg/cm^2	18 F/g (1 A/g)	[37]
Hollow carbon nanoplates	PIL	1.0 M Li_2SO_4	1 mg/cm^2	84 F/g (1 A/g)	
	PVDF			77 F/g (1 A/g)	[17]
Hollow carbon-MoS_2-carbon nanoplates	PVDF	1.0 M Li_2SO_4	0.5 mg/cm^2	178 F/g (1 A/g)	This work
			1 mg/cm^2	163 F/g (1 A/g)	

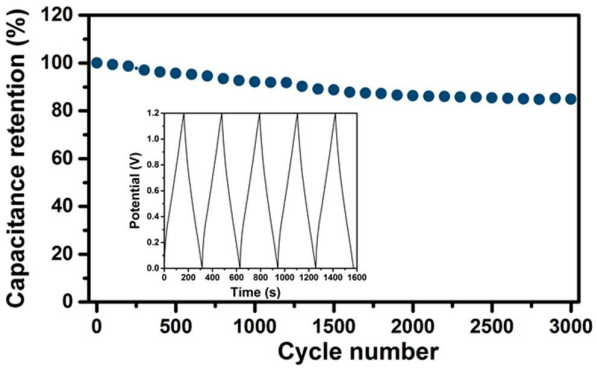

Figure 8. The cyclic performance of the symmetric supercapacitor. (Inset is the charge/discharge profile of the last five cycles)

values of various nanostructured MoS_2 materials of the literature, obtained in aqueous electrolytes. In comparison, our hollow carbon-MoS_2-carbon show higher specific capacitance than that of pure hollow carbon nanoplates and that of MoS_2 hollow spheres[10] and sponge materials,[36] and is comparable to the 2D layered MoS_2-rGO hybrids.[10] When increasing the mass loading on the electrode from 0.5 mg/cm^2 to 1 mg/cm^2, the specific capacitance only slightly decreases to 163 F/g at a current density of 1 A/g. This can be ascribed to the following features. (i) The hollow nanoplate structure could not only contribute more active sites for reaction, but act as ion-buffering reservoirs to shorten the ionic diffusion distance to the interior surface, promoting highcapability and avoiding volume expansion.[38] (ii) The carbon layers could support efficient electron transport of electrolyte towards MoS_2, resulting in a higher capacitance.

When calculated from the CV curves, the gravimetric capacitance of the hollow carbon-MoS_2-carbon nanoplates can reach 215 F/g (0.11 F/cm^2 in areal capacitance) at the scan rate of 10 mV/s as shown in Figure 7(a). The high capacity and rate capability is attributed to the hollow nanoplate structure and morphology of the hollow carbon-MoS_2-carbon nanoplates providing an easy intercalation mechanism of the electrolyte in- between the Van der Waals bonded MoS_2 layers together with a high specific surface area. The presence of the carbon coating should prevent the agglomeration of the MoS_2 sheets and improve the conductivity. Therefore, the hybrid material possesses more active sites for electrolyte ions than hollow carbon nanoplates as reported[17], leading to a superior capacitance of the material. Additionally, with the increase of the scan rate from 0.5 mV/s to 300 mV/s, the gravimetric capacitance value decreases from 303 F/g to 103 F/g, which may result from insufficient ion diffusion within a constant time that may take place at a high scan rate.[10, 39]

The energy density and power density values have been calculated from the CV curves according to eqs. (2) and (3), in Figure 7(b). The maximum energy density and power density of the material in our symmetric supercapacitor then could be calculated to 78 Wh/kg and 3806 W/kg, respectively. The energy density of our hollow carbon-MoS_2-carbon nanoplates are higher than that of pure hollow carbon nanoplates with the same electrode mass loading in supercapacitors.[17] The durability of the hollow carbon-MoS_2-carbon nanoplates is tested by galvanostatic charge-discharge at constant current density of 1 A/g as shown in Figure 8. The long time cycling stability is ensured by the fact that after 3000 charge-discharge cycles the specific capacitance could keep about 85% of the initial value, which is a little bit lower than that of the hollow carbon nanoplates based on electric double layer type mechanism (95%) reported by our group. This can be attributed to the dissolution in the electrolyte of a small part of our MoS_2 material, which can be triggered by dissolved oxygen and local pH variations that occur at both electrode/ electrolyte interfaces during cycling.[40]

Conclusions

The highly dispersible hollow sandwich-structured carbon-MoS_2-carbon nanoplates have been successfully synthesized and applied in supercapacitors with Li_2SO_4 aqueous solution as electrolyte. Using a multistep strategy, hollow carbon-MoS_2-carbon hybrid nanoplates were synthesized by the L-cysteine assisted hydrothermal method in the presence of sodium molybdate using gibbsite as the template and polydopamine as carbon precursor. After calcination and etching of the gibbsite template, uniform hollow platelets were obtained, which consist of a sandwich-like assembly of the partial graphitic carbon and the two-dimensional layered MoS_2 flakes. The presence of partial graphitic carbon coating on both sides of MoS_2 nanoplate improved the electrical conductivity and dispersibility of the hybrid material. The 2D hollow nanoplate morphology provided the material with high specific surface area of 543 m^2/g and pore size of 5.3 nm. The active electrode material exhibited nearly ideal capacitive behaviour at low frequencies, demonstrated good conductive capability and diffusion of the electrolyte ions in two electrode test cell. The hollow structure could not only provide more active sites for reaction, but prevent volume change during charging/discharging process. In symmetric two electrode configurations, it shows high specific capacitance of 248 F/g at constant 0.1 A/g current density and good electrochemical stability over 3000 cycles. By comparison, a hollow carbon material obtained using the same templating method (reported by our group) showed much lower electrochemical performance. This emphasizes the advantage of such a hybrid nanostructure that can benefit from both the electronic conductivity of the carbon and the high intrinsic electrochemical performance of MoS_2. The maximum energy density is calculated as 78 Wh/kg, which is higher than that of pure hollow carbon nanoplates. Its well-defined hollow sandwich structure, hexagonal shape and colloidal stability shows remarkable improvements in the synthesis of 2D nanomaterials and the application in energy storage, especially in aqueous systems. In addition, this well design structure could show significant advantages for many other applications, such as catalyst, optical applications and so on.

Experimental Section

Materials and methods

Materials. Aluminum isopropoxide (AIP, Sigma-Aldrich), hydrochloric acid, tetraethyl orthosilicate (TEOS, Sigma-Aldrich), 3-hydroxytyramine hydrochloride (dopamine, Sigma-Aldrich), aluminum sec-butoxide (ASB, Sigma-Aldrich), ammonia (Sigma-Aldrich), polyvinylpyrrolidone (PVP, 40,000 g/mol, Sigma-Aldrich), tris(hydroxymethyl) aminomethane (Tris, Sigma-Aldrich), ammonium hydrogen difluoride (NH_4HF_2, Sigma-Aldrich), lithium sulfate monohydrate (Sigma-Aldrich), polyvinylidene fluoride (PVDF, Sigma-Aldrich), Nafion (117, Sigma), Sodium molybdate (Na_2MoO_4, Sigma-Aldrich), L-cysteine (Sigma-Aldrich), HCl (37%, Sigma-Aldrich), and 1-methyl-2-pyrrolidinone (NMP, Sigma-Aldrich) were used as received. Ethanol (absolute) was purchased from VWR. Milli-Q water with a resistivity 18.2 MΩ•cm at 25 ℃ and a TOC<5 ppb was used in all preparations.

The synthesis process of hollow carbon-MoS_2-carbon is shown in Figure 1.

Synthesis of Gibbsite Nanoplates. The synthesis of gibbsite nanoplatelets follows the reference[17]. In a typical run, 0.08 mol/L ASB and 0.08 mol/L AIP were dissolved in 1.5 L of water, which was acidified with 11 mL HCl (37%). After mechanically stirring for 10 days, the mixture was heated in a polypropylene bottle in a water bath at 85 ℃ for 3 days. Then the sample was dialyzed against water for several days in regenerated cellulose tubes (MWCO 14000) until the conductivity reached 20 µS/cm. Finally, the colloidal dispersion was centrifuged to remove the small particles and dispersed in water for further use.

Synthesis of Gibbsite-PDA nanoplates. The coating of gibbsite nanoplatelets with a polydopamine shell was carried out by a self-oxidation polymerization method. In this work, 50 mg gibbsite were dispersed into 100 mL of 0.5 mg/mL dopamine solution in air at pH 8.5 in 10 mM TRIS buffer. After two hours of ultrasonication to avoid the aggregation of particles, the solution was stirred overnight. Then the polydopamine-coated gibbsite nanoplates were washed by deionized water several times until the supernatant solution became clear.

Synthesis of Gibbsite-PDA-MoS_2 nanoplates. A thin layer of MoS_2 was coated onto the gibbsite-PDA nanoplates using a hydrothermal method.[8, 20] In a typical synthesis, 0.121 g Na_2MoO_4 were added to a 100 mL polydopamine-coated gibbsite suspension in water (0.5 mg/mL). After two minutes of stirring, 0.303 g L-cysteine was added to the solution which was sonicated for 30 minutes. After that, a certain amount of HCl (37%) was added drop by drop under stirring to adjust the pH to 2.3. The solution was then transferred to a 120 mL Teflon-lined autoclave, which was sealed, heated at 200 ºC for 24 hours, and naturally cooled down to room temperature afterwards. The obtained product was collected by centrifugation and washed several times with deionized water.

Synthesis of Gibbsite-PDA-MoS_2-PDA nanoplates. To obtain fully polydopamine–coated MoS_2 particles, the polydopamine deposition step was repeated as described above.

Synthesis of hollow carbon-MoS_2-carbon nanoplates. In order to avoid the aggregation of the nanoplates during carbonization of the polydopamine shells, silica was used to encapsulate the particles. The process was following. 1.14 mL HCl (37%) was added to 100 mL of Gibbsite-dopamine-MoS_2-dopamine dispersion in water. After 10 minutes of stirring followed by 10 minutes of ultrasonication, 8.56 mL TEOS were added in portions under the liquid surface of the mixture while stirring. The reaction was run overnight and then the final solution was freeze-dried. Afterwards, annealing and carbonization was performed at 700 ºC under argon for 3 hours to convert polydopamine to carbon. The gibbsite template and silica were removed with HCl (37%) and NH_4HF_2 (4M water solution), respectively. The final products were obtained after washing and freeze-drying.

Characterization

Transmission electron microscopy (TEM) and high-resolution transmission electron microscopy (HR-TEM) images were performed with a JEOL JEM-2100 instrument operated at an acceleration voltage of 200 kV.[41] X-ray diffraction (XRD, Bruker D8) measurements were conducted by using a monochromatized X-ray beam with Cu Kα radiation with 0.05°/min scan rate.[42] TGA (Perkin- Elmer Pyris 1) was carried out in the temperature range 25 - 680 °C at a heating rate of 10 °C/min in air. The Raman spectra were measured using a LabRAM HR Evolution Raman Spectrometer with a HeNe laser as the excitation line of 633 nm.[43]

Electrochemical measurements

Electrochemical measurements were firstly conducted in a three-electrode system to explore the working mechanism of the supercapacitor with hollow carbon-MoS_2-carbon nanoplates as an electrode material. For this part, 1M Li_2SO_4 was used as an electrolyte, an Ag/AgCl (saturated KCl) electrode and a platinum wire were used as reference and counter electrodes, respectively. 1 mg active material was mixed with 190 µL H_2O, 50 µL ethanol and 10 µL 5wt% Nafion under sonication for 20 minutes. Then, part of the mixture was drop casted on the surface of a glassy carbon electrode and was subsequently dried in air. Typically, a coating of 40 µg of hollow carbon-MoS_2-carbon nanomaterial on 0.077 cm^2 glassy carbon electrode was obtained.

For a symmetrical two-electrode test cell, the electrodes were fabricated by mixing the active material (hollow carbon-MoS_2-carbon), carbon black and PVDF in a 8:1:1 mass ratio in NMP by stirring overnight to obtain a slurry. This latter was then spread with a doctor-blade apparatus on an aluminum foil used as a current collector. The obtained homogeneous coating was subsequently dried overnight at 60 ºC in vacuum oven to remove the solvent. Aluminum foil supported electrode disks of 12 mm in diameter were cut out. The average mass loading of the one electrode was around 0.5 mg/cm^2. The cut out electrodes were dried at 120 ℃ for 48 h under vacuum before the each measurement. Thereafter, the symmetrical two-electrode test cell was assembled employing the 1.0 M Li_2SO_4 in H_2O as an electrolyte. Glass fiber was used as the separator. The assembled test cell was left for stabilization and wetting overnight before the electrochemical characterizations, i.e., to evaluate the capacitance and the stability.

All three-electrode electrochemical measurements were carried out with GAMRY Instruments (GAMRY Interface 1000) and all two-electrode system performance were measured with a Biologic electrochemical workstation (MPG2 galvanostat/potentiostat). Electrochemical characterizations were performed at room temperature.

The cyclic voltammetry (CV) tests were performed at various scan rates from 0.5 to 300 mV/s. The specific capacitance of the supercapacitor is first calculated from CV curves based on the equation (1)[10, 44]:

$$C_{sp-CV} = 2 \times \frac{\int I(V)dV}{\nu m \Delta V} \qquad (1)$$

Where $\int I(V)dV$ is the area of the CV closed curve, ν is the scan rate (V/s), m is the mass loading of the active material on the electrode (g), ΔV is the potential range (V).

Then the energy density (ED) and power density (PD) can be calculated using the following equations (2) and (3)[45]:

$$ED = \frac{1}{2} \times C_{sp}(\Delta V)^2 \qquad (2)$$

$$PD = \frac{1}{2} \times C_{sp}(\Delta V)v \qquad (3)$$

Galvanostatic charge/discharge (GCD) tests of the symmetric supercapacitor with hollow carbon-MoS_2-carbon nanoplates as electrode material at fixed currents from 0.1 to 5.0 A/g within the voltage range from 0 to 1.2 V were studied.

From the GCD cycling, the capacitance of the full supercapacitor can be calculated using equation (4):

$$C_{GC} = \frac{I \times \Delta t}{\Delta V \times m} \qquad (4)$$

Where C_{GC} is the gravimetric capacitance of the symmetric supercapacitor (F/g), I is the applied current (A), Δt corresponds to the discharging time (s), ΔV is the potential range (V) and m the total mass of active material of both electrodes (g).

Multiplying this latter value per 4 allows obtaining the gravimetric capacitance value of the hollow C-MoS_2-C material in the device as shown in equation (5):

$$C_{sp-GC} = 4 \times C_{GC} \qquad (5)$$

The same procedure was applied to obtain the areal capacitance of the device and the material, by replacing the mass values with the area of the electrodes.

The electrochemical impedance spectroscopy was performed within the frequency range from 20 kHz to 10 mHz at open circuit voltage. The recorded data were fitted using ZView software Version: 2.1c.

Acknowledgements

T.Q. gratefully acknowledges financial support of CSC scholarship. Kai Skrodczky (HU Berlin) is acknowledged for his help with the synthesis of MoS_2 and Raman spectra measurements. The authors also thank the Joint Lab for Structural Research at the Integrative Research Institute for the Sciences (IRIS Adlershof).

Keywords: highly dispersible • two-dimensional • MoS_2 • sandwich structure • supercapacitors

[1] a) T. Wang, S. Chen, H. Pang, H. Xue, Y. Yu, *Adv. Sci.* **2017**, *4*, 1600289; b) M. Zhang, Z. J. Huang, X. Wang, H. Y. Zhang, T. H. Li, Z. L. Wu, Y. H. Luo, W. Cao, *Sci. Rep.* **2016**, *6*, 11; c) J. Luxa, O. Jankovsky, D. Sedmidubsky, R. Medlin, M. Marysko, M. Pumera, Z. Sofer, *Nanoscale* **2016**, *8*, 1960-1967; d) D. Cao, H. B. Shu, T. Q. Wu, Z. T. Jiang, Z. W. Jiao, M. Q. Cai, W. Y. Hu, *Appl. Surf. Sci.* **2016**, *361*, 199-205; e) M. Moller, N. Tarabanko, C. Wessel, R. Ellinghaus, H. Over, B. M. Smarsly, *RSC Advances* **2018**, *8*, 132-144; f) P. Mei, Y. V. Kaneti, M. Pramanik, T. Takei, O. Dag, Y. Sugahara, Y. Yamauchi, *Nano Energy* **2018**, *52*, 336-344.

[2] a) Y. X. Huang, J. H. Guo, Y. J. Kang, Y. Ai, C. M. Li, *Nanoscale* **2015**, *7*, 19358-19376; b) M. Acerce, D. Voiry, M. Chhowalla, *Nat. Nanotechnol.* **2015**, *10*, 313-318.

[3] a) Y. C. Liu, L. F. Jiao, Q. Wu, Y. P. Zhao, K. Z. Cao, H. Q. Liu, Y. J. Wang, H. T. Yuan, *Nanoscale* **2013**, *5*, 9562-9567; b) D. W. Ma, W. W. Ju, T. X. Li, X. W. Zhang, C. Z. He, B. Y. Ma, Y. A. Tang, Z. S. Lu, Z. X. Yang, *Appl. Surf. Sci.* **2016**, *364*, 181-189; c) J. Liu, P. J. Lu, S. Liang, J. Liu, W. Wang, M. Lei, S. Tang, Q. Yang, *Nano Energy* **2015**, *12*, 709-724; d) Y. T. Lu, D. M. Chu, M. S. Zhu, Y. K. Du, P. Yang, *Phys. Chem. Chem. Phys.* **2015**, *17*, 17355-17361; e) L. Ma, L. M. Xu, X. P. Zhou, X. Y. Xu, *Mater. Lett.* **2014**, *132*, 291-294.

[4] L. David, R. Bhandavat, G. Singh, *ACS Nano* **2014**, *8*, 1759-1770.

[5] a) X. Zhang, Z. C. Lai, C. L. Tan, H. Zhang, *Angew. Chem. Int. Ed.* **2016**, *55*, 8816-8838; b) X. Huang, Z. Y. Zeng, H. Zhang, *Chem. Soc. Rev.* **2013**, *42*, 1934-1946; c) Z. Y. Zeng, Z. Y. Yin, X. Huang, H. Li, Q. Y. He, G. Lu, F. Boey, H. Zhang, *Angew. Chem. Int. Ed.* **2011**, *50*, 11093-11097; d) J. N. Coleman, M. Lotya, A. O'Neill, S. D. Bergin, P. J. King, U. Khan, K. Young, A. Gaucher, S. De, R. J. Smith, I. V. Shvets, S. K. Arora, G. Stanton, H. Y. Kim, K. Lee, G. T. Kim, G. S. Duesberg, T. Hallam, J. J. Boland, J. J. Wang, J. F. Donegan, J. C. Grunlan, G. Moriarty, A. Shmeliov, R. J. Nicholls, J. M. Perkins, E. M. Grieveson, K. Theuwissen, D. W. McComb, P. D. Nellist, V. Nicolosi, *Science* **2011**, *331*, 568-571.

[6] H. Matte, A. Gomathi, A. K. Manna, D. J. Late, R. Datta, S. K. Pati, C. N. R. Rao, *Angew. Chem. Int. Ed.* **2010**, *49*, 4059-4062.

[7] J. F. Xie, H. Zhang, S. Li, R. X. Wang, X. Sun, M. Zhou, J. F. Zhou, X. W. Lou, Y. Xie, *Adv. Mater.* **2013**, *25*, 5807-+.

[8] L. Zhang, H. B. Wu, Y. Yan, X. Wang, X. W. Lou, *Energy Environ. Sci.* **2014**, *7*, 3302-3306.

[9] P. Ilanchezhiyan, G. Mohan Kumar, T. W. Kang, *J. Alloy. Compd.* **2015**, *634*, 104-108.

[10] S. Kamila, B. Mohanty, A. K. Samantara, P. Guha, A. Ghosh, B. Jena, P. V. Satyam, B. K. Mishra, B. K. Jena, *Sci. Rep.* **2017**, *7*, 13.

[11] L. Ren, G. Zhang, Z. Yan, L. Kang, H. Xu, F. Shi, Z. Lei, Z. H. Liu, *ACS Appl. Mater. Interfaces* **2015**, *7*, 28294-28302.

[12] G. Wang, J. Zhang, S. Yang, F. X. Wang, X. D. Zhuang, K. Mullen, X. L. Feng, *Adv. Energy Mater.* **2018**, *8*, 8.

[13] a) W. Yang, L. He, X. C. Tian, M. Y. Yan, H. Yuan, X. B. Liao, J. S. Meng, Z. M. Hao, L. Q. Mai, *Small* **2017**, *13*, 8; b) B. C. Yang, C. X. Hao, F. S. Wen, B. C. Wang, C. P. Mu, J. Y. Xiang, L. Li, B. Xu, Z. S. Zhao, Z. Y. Liu, Y. J. Tian, *ACS Appl. Mater. Interfaces* **2017**, *9*, 44478-44484; c) T. H. Sun, X. H. Liu, Z. P. Li, L. M. Ma, J. Q. Wang, S. R. Yang, *New J. Chem.* **2017**, *41*, 7142-7150.

[14] S. Ishimoto, Y. Asakawa, M. Shinya, K. Naoi, *J. Electrochem. Soc.* **2009**, *156*, A563-A571.

[15] a) P. P. Wang, H. Y. Sun, Y. J. Ji, W. H. Li, X. Wang, *Adv. Mater.* **2014**, *26*, 964-969; b) L. Ye, W. Guo, Y. Yang, Y. F. Du, Y. Xie, *Chem. Mater.* **2007**, *19*, 6331-6337.

[16] M. Chen, Y. Dai, J. J. Wang, Q. Wang, Y. P. Wang, X. N. Cheng, X. H. Yan, *J. Alloy. Compd.* **2017**, *696*, 900-906.

[17] J. Cao, C. J. Jafta, J. Gong, Q. D. Rang, X. Z. Lin, R. Felix, R. G. Wilks, M. Bar, J. Y. Yuan, M. Ballauff, Y. Lu, *ACS Appl. Mater. Interfaces* **2016**, *8*, 29628-29636.

[18] H. Mao, L. Shi, S. L. Song, C. H. Xiao, J. Liang, B. T. Dong, S. J. Ding, *Inorg. Chem. Front.* **2017**, *4*, 1742-1747.

[19] J. M. Soon, K. P. Loh, *Electrochem. Solid State Lett.* **2007**, *10*, A250-A254.

[20] S. K. Park, S. H. Yu, S. Woo, B. Quan, D. C. Lee, M. K. Kim, Y. E. Sung, Y. Piao, *Dalton Trans.* **2013**, *42*, 2399-2405.

[21] K. Chang, W. X. Chen, *ACS Nano* **2011**, *5*, 4720-4728.

[22] a) R. Liu, S. M. Mahurin, C. Li, R. R. Unocic, J. C. Idrobo, H. J. Gao, S. J. Pennycook, S. Dai, *Angew. Chem. Int. Ed.* **2011**, *50*, 6799-6802; b) Y. Z. Song, Y. Song, H. Zhong, *Gold Bull.* **2011**, *44*, 107-111; c) S. Seok, I. Choi, K. G. Lee, B. G. Choi, K. J. Park, J. Y. Park, O. J. Kwon, S. J. Lee, D. H. Kim, *RSC Advances* **2014**, *4*, 42582-42584; d) M. Qiao, S. S. Meysami, G. A. Ferrero, F. Xie, H. Meng, N. Grobert, M. M. Titirici, *Adv. Funct. Mater.* **2018**, *28*, 7.

[23] S. Soll, T. P. Fellinger, X. C. Wang, Q. Zhao, M. Antonietti, J. Y. Yuan, *Small* **2013**, *9*, 4135-4141.

[24] D. Yang, R. F. Frindt, *J. Appl. Phys.* **1996**, *79*, 2376-2385.

[25] F. N. I. Sari, J. M. Ting, *Sci. Rep.* **2017**, *7*, 13.

[26] X. L. Zheng, J. B. Xu, K. Y. Yan, H. Wang, Z. L. Wang, S. H. Yang, *Chem. Mater.* **2014**, *26*, 2344-2353.

[27] a) A. C. Ferrari, *Solid State Commun.* **2007**, *143*, 47-57; b) X. B. Jin, R. He, S. Dai, *Chem. Eur. J.* **2017**, *23*, 11455-11459; c) A. C. Juhl, A. Schneider, B. Ufer, T. Brezesinski, J. Janek, M. Froba, *Beilstein J. Nanotechnol.* **2016**, *7*, 1229-1240.

[28] G. Chen, S. P. Wang, R. Yi, L. F. Tan, H. B. Li, M. Zhou, L. T. Yan, Y. B. Jiang, S. Tan, D. H. Wang, S. G. Deng, X. W. Meng, H. M. Luo, *J. Mater. Chem. A* **2016**, *4*, 9653-9660.

[29] G. Pickett, *J. Am. Chem. Soc.* **1945**, *67*, 1958-1962.

[30] E. P. Barrett, L. G. Joyner, P. P. Halenda, *J. Am. Chem. Soc.* **1951**, *73*, 373-380.

[31] W. Xu, T. Wang, S. D. Wu, S. Wang, *J. Alloy. Compd.* **2017**, *698*, 68-76.

[32] E. G. da Silveira Firmiano, A. C. Rabelo, C. J. Dalmaschio, A. N. Pinheiro, E. C. Pereira, W. H. Schreiner, E. R. Leite, *Adv. Energy Mater.* **2014**, *4*, 1301380.

[33] R. Zhou, C. J. Han, X. M. Wang, *J. Power Sources* **2017**, *352*, 99-110.

[34] a) X. W. Yang, C. Cheng, Y. F. Wang, L. Qiu, D. Li, *Science* **2013**, *341*, 534-537; b) E. R. Nightingale, *J. Phys. Chem.* **1959**, *63*, 1381-1387; c) P. Andalib, M. J. Wood, S. J. Korn, *J. Gen. Physiol.* **2002**, *120*, 739-755; d) X. M. Fan, C. Yu, J. Yang, Z. Ling, C. Hu, M. D. Zhang, J. S. Qiu, *Adv. Energy Mater.* **2015**, *5*, 7.

[35] a) K. C. Pham, D. S. McPhail, A. T. S. Wee, D. H. C. Chua, *RSC Advances* **2017**, *7*, 6856-6864; b) X. Z. Wu, W. Xing, L. Zhang, S. P. Zhuo, J. Zhou, G. Q. Wang, S. Z. Qiao, *Powder Technol.* **2012**, *224*, 162-167.

[36] S. K. Balasingam, M. Lee, B. H. Kim, J. S. Lee, Y. Jun, *Dalton Trans.* **2017**, *46*, 2122-2128.

[37] A. M. Liu, H. Lv, H. Liu, Q. G. Li, H. Zhao, *J. Mater. Sci. Mater. Electron.* **2017**, *28*, 8452-8459.

[38] a) Y. H. Dai, H. Jiang, Y. J. Hu, Y. Fu, C. Z. Li, *Ind. Eng. Chem. Res.* **2014**, *53*, 3125-3130; b) Y. Z. Li, Q. H. Zhang, J. X. Zhang, L. Jin, X. Zhao, T. Xu, *Sci. Rep.* **2015**, *5*, 10.

[39] a) K. Krishnamoorthy, S. J. Kim, *Mater. Res. Bull.* **2013**, *48*, 3136-3139; b) S. Ratha, C. S. Rout, *ACS Appl. Mater. Interfaces* **2013**, *5*, 11427-11433.

[40] Z. Y. Wang, A. von dem Bussche, Y. Qiu, T. M. Valentin, K. Gion, A. B. Kane, R. H. Hurt, *Environ. Sci. Technol.* **2016**, *50*, 7208-7217.

[41] H. Jia, R. Roa, S. Angioletti-Uberti, K. Henzler, A. Ott, X. Z. Lin, J. Moser, Z. Kochovski, A. Schnegg, J. Dzubiella, M. Ballauff, Y. Lu, *J. Mater. Chem. A* **2016**, *4*, 9677-9684.

[42] J. Cao, S. L. Mei, H. Jia, A. Ott, M. Ballauff, Y. Lu, *Langmuir* **2015**, *31*, 9483-9491.

[43] Y. Z. Jiang, N. Song, C. Wang, N. Pinna, X. F. Lu, *J. Mater. Chem. B* **2017**, *5*, 5499-5505.

[44] M. Sevilla, L. H. Yu, C. O. Ania, M. M. Titirici, *Chem. Electro. Chem* **2014**, *1*, 2138-2145.

[45] a) A. K. Samantara, S. C. Sahu, A. Ghosh, B. K. Jena, *J. Mater. Chem. A* **2015**, *3*, 16961-16970; b) Y. H. Lin, T. Y. Wei, H. C. Chien, S. Y. Lu, *Adv. Energy Mater.* **2011**, *1*, 901-907.

Entry for the Table of Contents

FULL PAPER

Text for Table of Contents

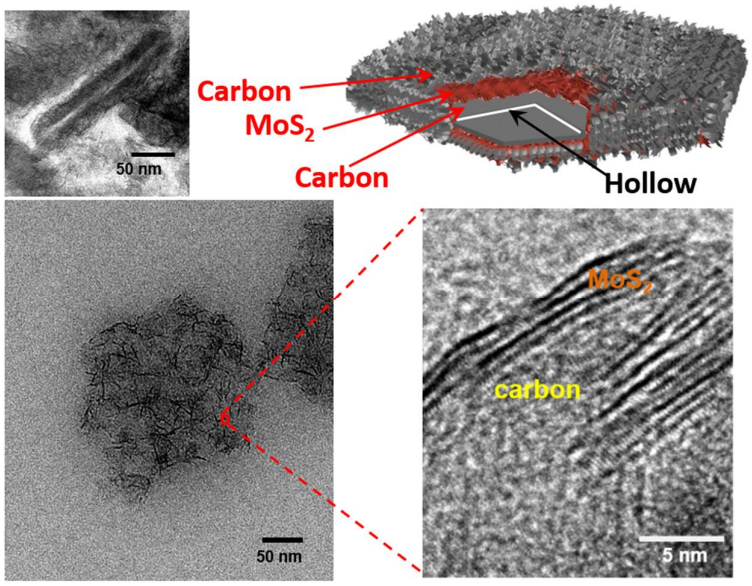

*Ting Quan, Nicolas Goubard-Bretesché, Eneli Härk, Zdravko Kochovski, Shilin Mei, Nicola Pinna, Matthias Ballauff, Yan Lu**

Page No. – Page No.

Highly Dispersible Hexagonal Carbon-MoS_2-Carbon Nanoplates with Hollow Sandwich Structures for Supercapacitors